Land Degradation & Development

WILEY

RESEARCH ARTICLE OPEN ACCESS

Heterogeneity and Controlling Mechanisms of Soil Organic Carbon Stocks Across Erosion Zones in China Under Future Climate Scenarios

Xinxin Jin[1] | Xintong Liu[1] | Qianlai Zhuang[2] | Zijiao Yang[1] | Zicheng Wang[1] | Chen Li[3] | Shuai Wang[1] | Yang Wang[4]

[1]College of Land and Environment, Shenyang Agricultural University, Shenyang, Liaoning Province, China | [2]Department of Earth, Atmospheric, and Planetary Sciences, Purdue University, West Lafayette, Indiana, USA | [3]Zhangwu County Agricultural Development Service Center, Fuxin, China | [4]College of Resources and Environment, Jilin Agricultural University, Changchun, Jilin Province, China

Correspondence: Shuai Wang (shuaiwang666@syau.edu.cn) | Yang Wang (wangyangsoil@jlau.edu.cn)

Received: 7 November 2025 | **Revised:** 11 March 2026 | **Accepted:** 9 July 2026

Keywords: future climate scenarios | soil erosion | soil organic carbon stocks | spatial heterogeneity

ABSTRACT

Soil organic carbon (SOC), as a key indicator of global carbon cycling and climate change response, plays a critical role in regional ecological security and agricultural sustainability. This study employs three machine learning models including the LightGBM, XGBoost, and random forest to simulate the spatial distribution of topsoil SOC stocks across different erosion types in China, and project their evolutionary trends under future climate scenarios. Model validation demonstrated high accuracy and strong consistency, while factor importance analysis revealed that mean annual temperature, mean annual precipitation, and elevation were the primary environmental drivers influencing the spatial variability of SOC stocks. Under both SSP245 and SSP585 scenarios, SOC stocks in China have a declining trend by 2050 and 2090. Areas affected by freeze–thaw erosion were the most sensitive to rising temperatures, whereas water erosion regions—due to their extensive spatial coverage—are projected to become the dominant zones of carbon loss. Spatially, carbon change hotspots were concentrated in the retreat zones of permafrost regions and mid- to low-latitude water erosion areas, while changes in wind erosion zones remain relatively moderate but were significantly influenced by shifts in precipitation patterns. This study highlights the regional heterogeneity in SOC stocks responses to future climate change across China, underscoring the necessity of integrating natural processes and human activities specific to each erosion type when formulating national-scale soil conservation and carbon management strategies. These findings provide a scientific foundation for promoting sustainable land management and enhancing ecosystem carbon sequestration capacity in China.

1 | Introduction

Soil organic carbon (SOC), as a central component of the global carbon cycle, plays an indispensable role in affecting climate change and sustaining ecosystem functions (Lal 2004; Naipal et al. 2018). In regions experiencing significant erosion, the erosion not only induces lateral transport and redistribution of carbon, but also modifies its biogeochemical cycling pathways (Lal 2003, 2005; Berhe et al. 2018; Zheng et al. 2025). As one of the countries most affected by soil erosion, China's extensive eroded areas provide a natural laboratory for investigating the resulting spatial heterogeneity of SOC (Gao et al. 2023). Due to variations in soil profile development, organic matter input pathways, and microbial community composition across areas with differing erosion intensities, the occurrence, stability, and turnover rate of SOC display pronounced spatial heterogeneity (de Nijs and Cammeraat 2020; Lin et al. 2022; Doetterl et al. 2025). A comprehensive understanding of this heterogeneous pattern is crucial for accurately assessing carbon budgets at the national scale, providing a scientific basis for developing targeted soil conservation strategies and advancing sustainable agricultural practices and carbon neutrality objectives.

Existing research has preliminarily elucidated the mechanisms by which erosion processes influence soil carbon dynamics through field observations and model simulations (Liu et al. 2003; Borrelli et al. 2021; Lin et al. 2022). A growing body of evidence indicates a non-linear relationship between erosion intensity and SOC stocks: mild erosion can enhance carbon sequestration and stabilize soil organic matter, whereas severe erosion typically results in net carbon loss (Lal 2005; Olson et al. 2016; Chappell et al. 2016). Studies have employed geostatistical methods and environmental factor interpolation to identify terrain undulations, vegetation cover, and land use patterns as key drivers influencing the spatial distribution of soil carbon in erosion-affected areas (Polyakov and Lal 2004; Olson et al. 2016; Wang, Zhang, et al. 2025). In typical erosion zones, these have demonstrated distinct soil carbon cycling patterns across varying erosion intensities: in depositional areas, carbon stabilization is primarily governed by physical protection mechanisms; whereas in strongly eroded areas, carbon mineralization processes are significantly enhanced (de Nijs and Cammeraat 2020; Lal 2005; Olson et al. 2016). These insights provide a critical theoretical foundation for understanding carbon dynamics in erosional environments.

However, current research still faces significant methodological challenges and cognitive gaps (Naipal et al. 2018; Hancock et al. 2019). Most findings are confined to regional scales and lack a systematic analysis of the spatial patterns of SOC stocks in erosion-affected areas at the national level (Maïga-Yaleu et al. 2013; Hancock et al. 2019; Hunter et al. 2024). Regarding predictive models, traditional approaches struggle to accurately capture the complex nonlinear relationships between soil carbon and environmental factors, particularly failing to adequately account for the moderating effects of varying erosion intensities on responses to climate change (Polyakov and Lal 2004; Naipal et al. 2018). More importantly, existing research predominantly focuses on the analysis of current conditions and largely fails to integrate next-generation climate scenarios—such as the SSP-RCP framework—into long-term projections of soil carbon dynamics, leading to substantial uncertainty in forecasting future changes (Naipal et al. 2018; Adeyeri et al. 2024). These limitations hinder the development of targeted adaptation strategies for regions facing varying erosion risks under a changing climate.

This study aims to systematically explore the spatial heterogeneity and control mechanisms of SOC stocks in erosion-prone regions of China under future climate scenarios. The specific research objectives include: (1) constructing a high-precision national-scale distribution map of SOC stocks; (2) simulating the spatiotemporal dynamics of SOC stocks in the 2050s and 2090s under SSP245 and SSP585 scenarios using machine learning models; and (3) identifying the key environmental drivers that govern soil carbon dynamics across different erosion intensity zones. This study will enhance understanding of the soil carbon cycle's response mechanisms under climate change, provide a scientific basis for large-scale carbon sink management and ecological security planning, and contribute to the sustainable use of land resources and carbon neutrality goals.

2 | Materials and Methods

2.1 | Study Area

China has a unique geographical environment, offering a representative model for investigating the dynamics of SOC stocks under the influence of multiple erosion processes (Guo et al. 2021). In terms of terrain, China presents a significant three-level ladder pattern, with an average altitude dropping sharply from over 4000 m on the Qinghai Tibet Plateau to below 200 m on the eastern plain (Guan 2025). This large height difference (from the highest point of Mount Everest at 8848 m to the lowest point of Lake Edin at −154.31 m) directly shapes the spatial differentiation pattern of erosion types: the water erosion areas are mainly distributed in the Northeast Plain with an annual precipitation of over 800 mm and the hilly areas south of the Yangtze River. The wind erosion area is concentrated in the northwest inland with an annual precipitation of less than 400 mm, among which the soil erosion area on the Loess Plateau covers an area of 300,000 km^2. The freeze–thaw erosion zone is mainly distributed in the Qinghai Tibet Plateau and surrounding high mountain areas with an annual average temperature below −1°C, with a permafrost area of approximately 1.59×10^6 km^2. The study area encompasses multiple climatic zones, with the average annual temperature varying from −5°C in the north to 25°C in the south, and average annual precipitation declining from over 1600 mm along the southeastern coast to less than 50 mm in the northwestern interior. This gradient in the distribution of water and heat not only governs the spatial patterns of erosive forces but also significantly influences the accumulation and transport of SOC stocks. China's comprehensive environmental gradient sequence and diverse erosion types create a natural laboratory for investigating soil carbon cycling under global change. This study examines the spatiotemporal dynamics of surface SOC stocks across different erosion zones in China and identifies the primary environmental drivers. The insights and methodologies generated can serve as valuable theoretical references for regions worldwide facing similar erosion challenges, including wind-eroded areas in Central Asia, permafrost regions in North America, and water-eroded regions in Southeast Asia. These findings hold significant scientific value for refining global terrestrial carbon cycle models and guiding carbon sequestration and sink enhancement efforts in degraded ecosystems.

2.2 | Soil Sampling Collection

The soil profile data used in this study were obtained from the National Science and Technology Basic Resource Survey Project "China Soil Series Survey and Compilation of China Soil Series" (Project No. 2008FY110600), led by Dr. Zhang at the Institute of Soil Science, Chinese Academy of Sciences, Nanjing. This project's outcomes were officially published in 2020 and systematically integrated nationwide field survey data collected during 2017–2018. We digitized the geographic coordinates, soil horizon characteristics, and soil physicochemical properties for

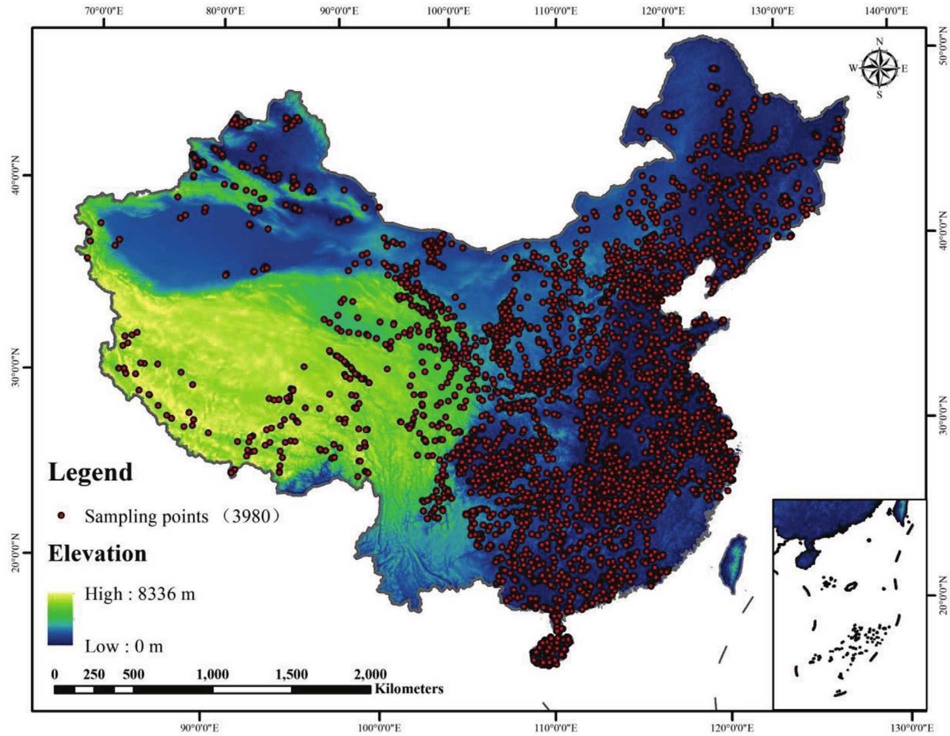

FIGURE 1 | Locations of sampling points overlaid with a 1 km resolution digital elevation model map of the study area. Wiley acknowledges that the borders within the figure are subject to multiple territorial claims. [Colour figure can be viewed at wileyonlinelibrary.com]

all sampling sites documented in the publication, and compiled a standardized dataset encompassing the entire territory of China, comprising 3800 complete soil profiles (Figure 1). The sampling locations were strategically determined by experts according to the principles of typicality and representativeness, and SOC was consistently measured using the dry combustion method (Matejovic 1993). To achieve an accurate estimation of surface SOC stocks, this study employed an equal-area spline function to continuously model the vertical distribution of SOC stocks within each soil profile. By fitting the depth-dependent variation curve and integrating it over the 0–30 cm depth range, the average carbon content of the entire topsoil layer could be reliably estimated. This method effectively addressed the comparability issue arising from inconsistent soil depth across different profiles, thereby enhancing the accuracy and reliability of SOC stocks estimation at regional scales (Odgers et al. 2012; Wang, Bian, et al. 2025). The detailed modeling procedure was described in Section 2.5.5 of this article. The construction and standardization of this high-quality dataset have established a robust foundation for in-depth analysis of soil carbon dynamics under various erosion types at the national scale.

2.3 | Environmental Factors

To effectively simulate the spatial distribution of SOC stocks across different soil erosion zones in China and identify the key environmental drivers underlying its spatial variability, this study selected nine representative factors from three major categories—topography, climate, and human activities: elevation (ELE), slope gradient (SG), slope aspect (SA), plan curvature (PC), catchment area (CA), topographic wetness index (TWI), mean annual precipitation (MAP), mean annual temperature (MAT), and land use type (LD). These factors were chosen due to their established influence on soil carbon dynamics through regulation of hydrological processes, microclimatic conditions, and vegetation productivity. Since the original data are derived from multiple sources, variations in spatial resolution and coordinate systems necessitate systematic preprocessing to ensure data consistency. Using the ArcGIS 10.2 platform, all raster data were resampled to a uniform spatial resolution of 1-km. Continuous factors were resampled using the bilinear interpolation method, whereas categorical data (e.g., land use) were processed using the nearest neighbor method to preserve their discrete class attributes. To minimize area distortion across China's extensive longitudinal range, all datasets were reprojected into the Albers equal-area conic projection. This standardized processing effectively ensures data consistency and enhances the spatial comparability required for subsequent statistical analysis and machine learning-based spatial simulation of SOC stocks. The 1-km resolution was selected to balance computational efficiency with the spatial scale of ecological processes influencing SOC stocks across multi-scale soil erosion regions in China.

2.3.1 | Topographic Factors

To systematically characterize the terrain-driven mechanisms influencing the spatial distribution of SOC stocks, this study derived six key terrain parameters—ELE, SG, SA, PC, TWI, and CA—from a 1-km resolution digital elevation model (DEM) sourced from the Geospatial Data Cloud platform of the Chinese Academy of Sciences. These parameters were selected due to their well-established roles in shaping soil formation, regulating hydrological processes, and supporting ecosystem functions (Blackburn et al. 2022).

ELE, as the primary topographic factor, exerts a profound influence on the accumulation and spatial distribution of SOC by modulating temperature regimes, hydrological processes, and biogeochemical cycles (Blackburn et al. 2022). SG and SA, as integrated terrain attributes, jointly regulate surface erosion intensity, local microclimatic conditions, and vegetation productivity, thereby shaping the spatial patterns of SOC (Adiyah et al. 2022). PC directly influences sediment transport and the redistribution of organic matter by reflecting zones of surface runoff acceleration and deceleration (Wang et al. 2023). TWI and CA collectively characterize the spatial variability of soil moisture. TWI, which integrates SG and upslope contributing area, is widely used to assess the potential for waterlogging (Wang, Zhang, et al. 2025), whereas CA reflects the control of drainage networks on subsurface flow pathways (Adhikari et al. 2019).

In terms of technical implementation, fundamental terrain parameters—including ELE, SG, SA, and PC—are derived using the spatial analysis module in ArcGIS 10.2. Hydrological terrain indices such as the TWI and CA are computed using SAGA GIS, a specialized terrain analysis tool capable of accurately processing DEM depressions and simulating hydrological flow paths. The selected topographic factors collectively form a multi-scale terrain representation system, effectively capturing the key controls of hydrological connectivity on SOC stocks distribution across slope to landscape scales.

2.3.2 | Climatic Factors

This study constructed a multi-period dataset (base year 2018, mid-2050s, and late 2090s) for two key climate variables—MAT and MAP—to systematically assess the potential impacts of climate change on SOC dynamics across different erosion zones. The base period data were obtained from observations at stations of the China Meteorological Administration and interpolated into a continuous grid surface with a spatial resolution of 1-km using the inverse distance weighting (IDW) method on the ArcGIS 10.2 platform, thereby ensuring a high-precision representation of regional climate characteristics. The future climate scenario data were obtained from the WorldClim platform and encompass two shared socioeconomic pathways—SSP245 (moderate emissions) and SSP585 (high emissions)—representing the 20-year average climatic conditions for the periods 2041–2060 and 2081–2100, respectively. These scenarios reflect potential climate trajectories under varying climate policies and socioeconomic development pathways. Among them, the SSP245 pathway represents moderate radiative forcing (approximately $4.5\,\mathrm{W\,m^{-2}}$), reflecting a stabilization scenario with moderate greenhouse gas mitigation efforts; in contrast, the SSP585 pathway reflects a future trajectory of increased reliance on fossil fuels, resulting in radiative forcing reaching ~$8.5\,\mathrm{W\,m^{-2}}$ by the end of the century, indicating a significantly more intense warming trend (Haghighi et al. 2025; Wang, Zhang, et al. 2025). This dataset integrates observational and simulated data at a consistent spatial resolution of 1 km, thereby enhancing the comparability of climatic factors across multiple time periods and providing a robust foundation for investigating the response mechanisms of the grassland carbon cycle to climate change in China, as well as for developing climate adaptation strategies. It holds significant scientific foresight and practical application value.

2.3.3 | Human Activity Factors

LD change serves as a critical indicator reflecting the impact of human activities on land systems. Since the Industrial Revolution, the pace of transformation has accelerated markedly, with the global annual land conversion rate rising from 0.3% before 1750 to 1.2% after 1850 (Naipal et al. 2018). Existing research indicates that ~$48.7 \pm 3.5\%$ of the global ice-free land surface has been substantially altered by human activities (Blackburn et al. 2022). To quantify the potential impact of human activities on the study area, this study utilizes 1-km resolution LD data for the year 2018 from the Resource and Environmental Science Data Center (RESDC) of the Chinese Academy of Sciences. The classification system adheres to the Technical Regulations for the Third National Land Survey (GB/T 21010–2017), comprising six primary categories: (1) cultivated land (including dry land and paddy fields), (2) forest land (defined as areas with canopy density > 0.2), (3) grassland, (4) construction land (characterized by an impervious surface ratio $> 50\%$), (5) wetland (encompassing rivers, lakes, and reservoirs), and (6) wasteland (with vegetation coverage $< 30\%$). According to appendix B of the ISO 19144-2:2012 standard, each land type is assigned a standardized numerical code ranging from 1 to 6 to enhance the interoperability of geographic computations and the reproducibility of spatial analyses. This classification system features a clear hierarchical structure and mutual exclusivity between classes, thereby supporting consistent recognition of landscape dynamics and enhancing compatibility with international environmental change model frameworks, thus providing a reliable spatial data foundation for studies on human–nature coupled systems.

2.4 | Soil Erosion Data

The spatial distribution data of soil erosion types in China were obtained from the official website of the Resource and Environmental Sciences and Data Center, Chinese Academy of Sciences (https://www.resdc.cn/data). The dataset was generated through a comprehensive and systematic approach that integrates multi-source geospatial information with specialized models, enabling the classification of soil erosion across China into three primary types: water erosion, wind erosion, and freeze–thaw erosion. The assessment of hydraulic erosion is primarily based on the Revised Universal Soil Loss Equation (RUSLE), which integrates factors such as rainfall erosivity, soil erodibility, slope length and steepness, vegetation cover, and conservation practices to estimate soil loss caused by rainfall and surface runoff. Wind erosion mapping typically employs models like the Revised Wind Erosion Equation (RWEQ), which incorporates key parameters including surface wind speed, soil moisture, surface roughness, vegetation coverage, and the content of erodible particles to simulate the detachment and transport of soil by wind. For freeze–thaw erosion, the definition primarily depends on terrain information derived from high-resolution DEM data (e.g., slope and aspect), freeze–thaw cycle characteristics identified through long-term remote sensing-based surface temperature inversion products, and integrated discrimination incorporating vegetation coverage conditions. Finally, within a unified GIS platform, evaluation results for these three erosion types were integrated, fused, and logically validated to produce a comprehensive spatial distribution map. This map indicates that water erosion is predominantly distributed in the eastern monsoon region and the Loess Plateau, wind erosion prevails in the northern arid and semi-arid regions, and freeze–thaw erosion is concentrated in high-altitude mountainous and plateau areas such as the Qinghai Tibet Plateau region in China. This achievement clearly demonstrates the intrinsic relationship between soil erosion types and natural geographical patterns in China, offering essential scientific data to support the development of zonal and classified ecological governance and protection strategies.

2.5 | Prediction Models

2.5.1 | eXtreme Gradient Boosting

eXtreme Gradient Boosting (XGBoost) is an efficient gradient boosting decision tree algorithm proposed by Chen et al. (2015). This model is essentially an optimized implementation based on the traditional gradient boosting framework, which integrates multiple weak learners (usually CART regression trees) to construct a powerful prediction model (Carmona et al. 2019). The core idea is to generate decision trees sequentially, with each tree dedicated to correcting the prediction error of the previous tree and gradually reducing the loss function through superposition learning (Chen et al. 2015). The core advantages of XGBoost are evident in several key aspects. First, it employs second-order Taylor expansion to optimize the loss function and incorporates a regularization term to control model complexity, thereby effectively mitigating the risk of overfitting (Sibindi et al. 2023). Second, the algorithm enables parallel processing: although tree construction is sequential, feature selection and split point computation can be performed in parallel, significantly enhancing computational efficiency (Carmona et al. 2019). Furthermore, XGBoost features an intrinsic mechanism for handling missing values by automatically learning the optimal splitting direction for such instances (Chen et al. 2015). It also supports a wide range of objective functions and evaluation metrics, making it adaptable to diverse tasks including classification, regression, and ranking. Owing to these strengths, XGBoost has demonstrated superior performance in numerous machine learning competitions and real-world industrial applications, establishing itself as one of the most widely adopted ensemble learning algorithms today (Chen et al. 2015; Carmona et al. 2019).

This study implemented the algorithm in R language (R Development Core Team 2013) using the "xgboost" package. The modeling process typically consists of three stages: data preparation, model training, and predictive evaluation. During data preparation, the dataset is converted into DMatrix format—an optimized data structure specifically designed for XGBoost to enhance computational efficiency. Model training is performed using the xgb.train function, where key parameters must be configured: eta (learning rate, which controls the contribution weight of each tree), max_depth (maximum tree depth, regulating model complexity), subsample (ratio of samples used for training each tree), colsample_bytree (ratio of features sampled per tree), min_child_weight (minimum sum of instance weights required in a leaf), gamma (minimum loss reduction threshold for splitting a node), lambda and alpha (L2 and L1 regularization terms), and nrounds (number of boosting iterations, i.e., number of trees). Additionally, the objective parameter must be specified to define the learning task—for example, "reg:squarederror" for regression tasks and "binary:logistic" for binary classification. To prevent overfitting and determine the optimal number of iterations, cross-validation can be conducted via the xgb.cv function. A comprehensive modeling workflow should also incorporate hyperparameter tuning, feature importance assessment, and model diagnostics to fully exploit the predictive power of XGBoost.

2.5.2 | Light Gradient Boosting Machine

Light Gradient Boosting Machine (LightGBM) is a high-performance gradient boosting decision tree framework (Ke et al. 2017). Like XGBoost, it belongs to the Boosting family within ensemble learning, but its primary design objective is to improve training efficiency and reduce memory consumption in large-scale data scenarios (Hindarto 2024). To achieve this, LightGBM employs two key techniques: first, Gradient-based One-Side Sampling (GOSS), which retains instances with large gradients while randomly sampling those with small gradients, thereby significantly reducing computational cost without compromising model accuracy (Guo et al. 2023); second, Exclusive Feature Bundling (EFB), which combines mutually exclusive features—those rarely non-zero simultaneously—in sparse datasets, effectively lowering feature dimensionality and memory usage (Hindarto 2024). These innovations enable LightGBM to train substantially faster than many comparable algorithms when handling high-dimensional and large-scale data (Ke et al. 2017). The primary advantages of LightGBM include rapid training speed, low memory usage, efficient handling of large-scale datasets, and accuracy that is comparable to or sometimes superior to that of XGBoost (Ke et al. 2017; Hindarto 2024). However, it has certain limitations: it may be prone to overfitting on small datasets due to its leaf-wise tree growth strategy, which can result in deeper trees despite high computational efficiency (Guo et al. 2023). Furthermore, LightGBM is more sensitive to parameter tuning, particularly those parameters associated with overfitting control.

This study employs the LightGBM package in R language (R Development Core Team 2013) to implement the model. The procedure typically involves installing and loading the package, followed by converting the data into the LightGBM-specific lgb.Dataset format. Model training is conducted using the lgb.train function, which requires careful configuration of several key parameters. These include: objective (specifying the task type, such as "regression" for regression or "binary" for binary classification), metric (evaluation metric, such as "l2" for regression or "AUC" for classification), boosting (set to "gbdt"), num_leaves (a critical parameter controlling model complexity due to leaf-wise splitting, typically set higher than the tree depth), learning_rate (step size shrinkage to prevent overfitting), feature_fraction (ratio for feature subsampling), bagging_fraction (ratio for data subsampling), and min_data_in_leaf (minimum number of data instances per leaf, crucial for preventing overfitting). Tuning these parameters via cross-validation and grid search is essential for constructing a high-performance LightGBM model.

2.5.3 | Random Forest

Random forest (RF) is a powerful ensemble learning algorithm introduced by statistician Breiman at the University of California, Berkeley in 2001. It belongs to the Bagging category of ensemble methods and operates by constructing a large number of decision trees and aggregating their predictions through majority voting for classification tasks or averaging for regression tasks, thereby achieving a more stable and accurate model (Wiesmeier et al. 2011). The term "random" is reflected in two key aspects: first, data randomness, achieved through Bootstrap sampling to generate diverse training subsets for individual trees; second, feature randomness, where at each node split, the optimal splitting feature is selected only from a randomly chosen subset of all available features (Nabiollahi et al. 2019). This dual randomness enhances the diversity among the trees, reduces model variance, increases robustness to noisy data, and ultimately improves generalization performance.

The most prominent advantages of random forests include: extremely high fault tolerance and resistance to overfitting, achieved through averaging the outputs of multiple decision trees (Breiman 2001); ease of implementation and tuning, as the algorithm is relatively insensitive to parameter choices and often yields strong performance without extensive hyperparameter optimization; the ability to naturally assess feature importance, providing an intuitive basis for feature selection (Wiesmeier et al. 2011); and the capacity to handle high-dimensional data without requiring extensive preprocessing, such as feature scaling, due to its inherent insensitivity to variable magnitude (Nabiollahi et al. 2019). However, several limitations exist: overfitting may still occur in the presence of highly noisy data; model interpretability is reduced compared with a single decision tree, making it more akin to a "black box"; and training a large ensemble of trees can demand substantial computational resources and time (Wiesmeier et al. 2011).

The most widely used and powerful package for implementing random forest in R language (R Development Core Team 2013) is randomForest. Model training can be accomplished using its core function randomForest (Nabiollahi et al. 2019). When calling this function, several key parameters must be configured: ntree specifies the number of decision trees in the forest—increasing the number enhances model stability but also raises computational cost (Wiesmeier et al. 2011); mtry controls feature randomness by determining the number of features randomly sampled at each node split (Nabiollahi et al. 2019). The choice of mtry significantly influences model performance, with smaller values promoting greater tree diversity (Wiesmeier et al. 2011); nodesize sets the minimum number of samples required in a terminal node, and larger values help prevent overfitting by limiting tree depth, thus serving as a regularization mechanism and simplifying the model structure (Nabiollahi et al. 2019). Additionally, users need only specify the prediction formula via the formula argument and provide the dataset, after which the function automatically performs model training. Feature importance can be obtained through the importance parameter, making the package highly convenient and efficient to use.

2.5.4 | Space-For-Time Substitution Method

Soil formation and evolution are governed by the complex interplay of multiple environmental drivers, primarily including parent material, climatic conditions, biological activity, topographic features, and temporal factors (McBratney et al. 2003). The "SCORPAN" model proposed by McBratney et al. (2003) provides a theoretical framework for analyzing spatial patterns of soil properties across different temporal scales. Recent developments in pedogenic modeling have integrated space-for-time substitution techniques (Adhikari et al. 2019), allowing researchers to simulate future soil conditions by adjusting climate, vegetation, and anthropogenic factors within the model structure. This approach has proven effective across various geographical regions—such as tropical ecosystems in Brazil, arid zones in Australia, and temperate landscapes in North America—particularly in projecting SOC dynamics under different environmental change scenarios (Adhikari et al. 2019; Wang, Zhang, et al. 2025; Wang, Bian, et al. 2025). However, the predictive reliability of these models is limited by inherent uncertainties arising from the lack of observational data for future environmental conditions (Reyes Rojas et al. 2018; Wang, Bian, et al. 2025). In the context of China, this study utilized comprehensive soil profile datasets collected from 2018 to investigate the correlations between SOC stocks within a depth range of 0–30 cm and various environmental parameters. The analytical approach was grounded on the premise that lithogenic factors, biotic components, and landscape morphology would remain relatively stable within the projected timeframe, allowing for the isolation of climate and land use effects through space-for-time substitution. While this assumption entails certain methodological limitations, particularly concerning long-term ecological feedback mechanisms, it nonetheless provides valuable insights into the dynamics of soil carbon and nitrogen pools under varying climate and land management scenarios, offering significant implications for understanding alpine ecosystem responses to global change.

2.5.5 | Equal-Area Spline Profile Function

The equal-area spline profile function was proposed (Bishop et al. 1999) and is a key mathematical tool for modeling the vertical distribution of soil profile attributes. This method achieves accurate depth-wise fitting of soil parameters across different stratigraphic layers by constructing continuous and smooth spline curves (Odgers et al. 2012). The core theoretical advantage stems from the incorporation of equal-area constraints, which ensure that the integrated area over each fitting interval strictly matches the total attribute value of the corresponding measured layer (Bishop et al. 1999). This effectively mitigates the area distortion commonly encountered in traditional interpolation methods during interlayer inference (Bonfatti et al. 2016). This model requires setting only two parameters: the number of nodes and the smoothing coefficient λ (Odgers et al. 2012). The number of nodes is typically determined according to the hierarchical structure of soil genesis, whereas λ controls the trade-off between the fidelity of the fitted curve to the observed data and its smoothness. A small λ may lead to overfitting of sampling noise, while an excessively large λ can obscure important profile shape features (Bishop et al. 1999). Although this function offers significant advantages in characterizing the nonlinear vertical variation of soil properties, its fitting performance heavily relies on the accuracy and completeness of profile layer data and may be compromised under conditions of low sampling density or incomplete layer information (Bonfatti et al. 2016).

To optimize the model performance in this study, five values of λ (0.0001, 0.001, 0.01, 0.1, and 1) were systematically evaluated. The results demonstrated that the root mean square error reached its minimum at $\lambda = 0.1$, indicating that this parameter setting enabled the model to achieve an optimal balance between fitting accuracy and generalization capability. All equal-area spline profile function fitting operations are conducted using SplineTool V2 (ASRIS 2011), developed by the Commonwealth Scientific and Industrial Research Organisation of Australia, which offers a robust and standardized platform for continuous profiling data processing and modeling. The equal-area spline profile function converts discrete layered observations into continuous depth profiles, offering a methodological foundation for estimating soil carbon stocks and advancing the theoretical shift in digital soil mapping from discrete layer-based aggregation to continuous vertical representation.

2.6 | Model Validation

The primary objective of this study was to systematically evaluate and compare the performance of three mainstream machine learning models—XGBoost, LightGBM, and RF—in predicting SOC stocks in topsoil (0–30 cm) within eroded regions of China, with the aim of identifying the most suitable modeling approach. To ensure robustness and comparability in model evaluation, a 10-fold cross-validation strategy was employed, and multiple performance metrics—including mean absolute error (MAE), root mean square error (RMSE), coefficient of determination (R^2), and Lin's concordance correlation coefficient (LCCC) (Lin 1989)—were comprehensively utilized. Given the inherent randomness in the training processes of these models, 100 independent iterations were conducted for each to yield stable and reliable predictions. The calculation methods for each evaluation metric are as follows:

$$\mathrm{MAE} = \frac{1}{n}\sum_{i=1}^{n}\left|a_i - b_i\right| \tag{1}$$

$$\mathrm{RMSE} = \sqrt{\frac{1}{n}\sum_{i=1}^{n}\left(a_i - b_i\right)^2} \tag{2}$$

$$R^2 = \frac{\sum_{i=1}^{n}\left(a_i - \bar{b}\right)^2}{\sum_{i=1}^{n}\left(b_i - \bar{b}\right)^2} \tag{3}$$

$$\mathrm{LCCC} = \frac{2r\sigma_a\sigma_b}{\sigma_a^2 + \sigma_b^2 + \left(\bar{a} - \bar{b}\right)^2} \tag{4}$$

In the formula, a_i and b_i represent the predicted and measured values of the i-th sample, respectively; n is the total number of samples; $\bar{a}$ and $\bar{y}$ are the average values of predicted and measured values, respectively; r is the pearson correlation coefficient between the predicted value and the measured value; σ_a and σ_b are the variances of the predicted and measured sets, respectively.

3 | Results

3.1 | Descriptive Statistics

Table 1 presented the basic statistical characteristics of various environmental factors. The mean SOC stocks are 15.84 t/ha, with a standard deviation of 17.73, indicating high variability in the data. The skewness (6.26) and kurtosis (62.39) values revealed

TABLE 1 | Statistical analysis of surface soil organic carbon stocks (0–30 cm) and associated environmental factors based on 3800 sampling points.

Property	Unit	Min.	Max.	Mean	SD	Ske.	Kur.
SOC stocks	t ha	0.01	290.01	15.84	17.73	6.26	62.39
ELE	m	−151.55	5440.84	773.54	1071.95	2.10	4.19
SG	Degree	0.00	25.88	2.01	3.02	2.78	9.82
SA	Degree	−1.00	359.98	171.75	108.08	0.11	−1.27
PC	Index	−0.06	0.07	0.00	0.01	0.22	13.82
TWI	Index	6.54	15.26	11.16	2.02	0.04	−0.91
CA	$m^2 m^{-1}$	1.15×10^6	10955.3×10^6	333.36×10^6	595.8×10^6	6.00	62.58
MAP	mm	16.52	3362.43	1017.32	644.98	0.66	−0.52
MAT	Degree celsius	−6.21	26.74	12.79	6.89	−0.32	−0.76

Abbreviations: CA, catchment area; ELE, elevation; Kur., kurtosis; MAP, mean annual precipitation; MAT, mean annual temperature; Max., maximum; Min., minimum; PC, plan curvature; SA, slope aspect; SG, slope gradient; Ske., skewness; TWI, topographic wetness index.

TABLE 2 | Pearson correlation coefficients between surface soil organic carbon stocks (0–30 cm) and environmental factors derived from 3800 sampling points.

Property	SOC stocks	ELE	SG	SA	PC	TWI	CA	MAP	MAT
ELE	0.23**								
SG	0.19**	0.39**							
SA	0.02	−0.05**	−0.01						
PC	−0.01	0.04**	0.12**	0.01					
TWI	−0.19**	−0.44**	−0.72**	−0.01	0.01				
CA	−0.06**	−0.11**	−0.29**	−0.03	0.01	0.49**			
MAP	0.05**	−0.37**	0.07**	0.06**	0.02	−0.18**	−0.35**		
MAT	−0.21**	−0.57**	−0.11**	0.04*	−0.01	0.07**	−0.18**	0.75**	
LD	0.04*	0.30**	0.07**	−0.05**	0.03*	−0.03	0.07**	−0.20**	−0.24**

Abbreviations: CA, catchment area; ELE, elevation; LD, land use; MAP, mean annual precipitation; MAT, mean annual temperature; PC, plan curvature; SA, slope aspect; SG, slope gradient; TWI, topographic wetness index.
*$p < 0.05$.
**$p < 0.01$.

that the SOC stocks distribution was strongly right skewed and highly peaked, suggesting a non-normal distribution. ELE ranged from −151.55 m to 5440.84 m, with a mean of 773.54 m and a large standard deviation of 1071.95, reflecting substantial topographic variation across the study area. The mean SG and SA were 2.01° and 171.75°, respectively. A relatively high skewness value for slope (2.78) indicated that most areas have gentle slopes, although steep-slope outliers were present. PC had a mean close to zero and a symmetrically distributed dataset; however, the kurtosis value of 13.82 suggested a high concentration of data around the mean. The average TWI was 11.16, with near-normal distribution (skewness = 0.04, kurtosis = −0.91). CA varied widely, ranging from 1.15×10^6 to $10955.3 \times 10^6\, m^2/m$, with a skewness of 6.00, indicating the presence of extreme positive outliers. MAP and MAT were 1017.32 mm and 12.79°C, respectively, both exhibiting approximately symmetric distributions.

Table 2 showed the Pearson correlation coefficient matrix among all variables. SOC stocks exhibited significant positive correlations with ELE and SG ($r = 0.23$ and $r = 0.19$, respectively), and significant negative correlations with TWI and MAT ($r = -0.19$ and $r = -0.21$, respectively), indicating that higher elevation and steeper slopes were associated with greater SOC accumulation, whereas more humid conditions and elevated temperatures might inhibit SOC stocks. ELE was significantly correlated with multiple variables, showing strong negative associations with TWI ($r = -0.44$) and MAT ($r = -0.57$), highlighting its critical role in modulating hydrothermal regimes. MAP and MAT were highly positively correlated ($r = 0.75$), suggesting a coupled variation in moisture and thermal conditions.

3.2 | Model Performance and Prediction Uncertainty

Based on the model performance evaluation results presented in Table 3 and the spatial distribution standard deviation (SD) of the predicted values shown in Figure 2a, the predictive accuracy and uncertainty of the three machine learning models across different erosion types could be comprehensively assessed. In terms of predictive performance, the LightGBM model demonstrated superior accuracy across most erosion types, achieving R^2 values of 0.66 for water erosion, 0.66 for wind erosion, and 0.67 for freeze–thaw erosion—consistently outperforming other models in these categories. Moreover, its relatively low RMSE and MAE values further confirm high prediction precision. The XGBoost and RF models also exhibited strong predictive capabilities, with LCCC exceeding 0.8 between each model pair, indicating a high degree of consistency between predicted and observed values. Regarding uncertainty quantification, Figure 2a displayed the spatial variability of model predictions using SD, where higher SD values correspond to greater prediction uncertainty—potentially due to sparse data coverage, complex environmental interactions, or variable model sensitivity to local features. For instance, freeze–thaw erosion showed

TABLE 3 | Statistical analysis of model prediction performance across different erosion zones.

Erosion type	Model	R^2	RMSE	MAE	LCCC
Water erosion	XGBoost	0.59	10.33	5.82	0.8
	LightGBM	0.66	9.41	4.76	0.84
	RF	0.61	10.12	4.85	0.83
Wind erosion	XGBoost	0.62	9.52	4.12	0.86
	LightGBM	0.66	9.72	3.61	0.84
	RF	0.64	10.06	4.28	0.84
Freeze–thaw erosion	XGBoost	0.61	22.29	13.93	0.85
	LightGBM	0.67	20.37	13.67	0.85
	RF	0.65	21.01	14.06	0.87

Abbreviations: LCCC, Lin's concordance correlation coefficient; LightGBM, Light Gradient Boosting Machine; MAE, mean absolute error; R^2, coefficient of determination; RF, Random forest; RMSE, root mean square error; XGBoost, eXtreme Gradient Boosting.

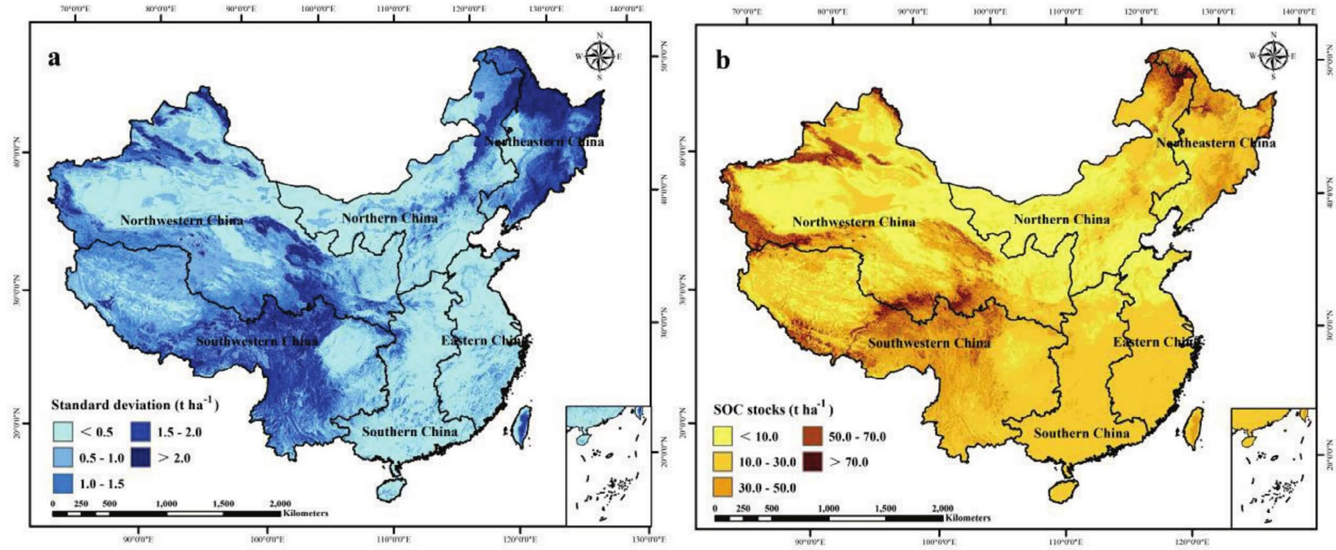

FIGURE 2 | Maps of average standard deviation (a) and spatial distribution (b) derived from 100 iterations of the LightGBM model. Wiley acknowledges that the borders within the figure are subject to multiple territorial claims. [Colour figure can be viewed at wileyonlinelibrary.com]

relatively high RMSE values (e.g., 20.37 for LightGBM), and when combined with its widespread SD distribution, this reflected substantial variability and uncertainty in modeling such processes. In contrast, water and wind erosion models yielded lower RMSE and MAE values, suggesting smaller SD magnitudes and consequently more stable and reliable predictions. In summary, although each model has demonstrated reliable predictive performance across various erosion types, associated uncertainties remain significant—particularly in regions characterized by high environmental heterogeneity. Future efforts should focus on integrating additional auxiliary data or adopting ensemble modeling approaches to enhance model robustness and predictive accuracy.

3.3 | Relative Importance of Environment Factors Across Erosion Zones

In the process of water erosion, MAT (27.84%) and MAP (16.23%) were the dominant environmental factors influencing SOC stocks, highlighting the key role of hydrothermal conditions in regulating SOC dynamics in water-eroded regions. Additionally, ELE and PC exerted significant effects, indicating that topographic characteristics indirectly shape SOC stocks distribution by modulating surface runoff and soil retention capacity. In wind-eroded environments, MAP (42.91%) was the most influential factor, emphasizing the critical importance of water availability for SOC accumulation and stability. MAT and CA followed in importance, suggesting that both climatic and topographic factors jointly regulate carbon cycling under wind erosion. In freeze–thaw erosion systems, MAP (48.20%) had the highest explanatory power, further underscoring the central role of precipitation—likely through its influence on snow cover, soil moisture, and freeze–thaw frequency—in these environments. MAT and ELE also significantly influenced SOC dynamics, demonstrating that thermal regimes and altitudinal gradients affected SOC stability by altering the intensity and duration of freeze–thaw cycles.

3.4 | Spatial Heterogeneity of Soil Organic Carbon Stocks Across Erosion Zones

According to Table 4 and Figure 3, different types of erosion zones exhibited significant spatial heterogeneity and dynamic changes in topsoil SOC stocks under the baseline period (2018) and future climate change scenarios, reflecting the complexity of environmental driving and climate response. During the baseline period, there were significant differences in SOC stocks among the three erosion zones: the freeze–thaw erosion zone had the highest SOC stocks (33.69 t ha^{-1}), followed by the water erosion zone (20.53 t ha^{-1}), and the wind erosion zone had the lowest (10.47 t ha^{-1}), reflecting the synergistic control of temperature, moisture, and erosion mechanisms on carbon accumulation. From the perspective of spatial distribution (see attached figure), high SOC stocks areas were mainly distributed in high-altitude areas with strong freeze–thaw effects and humid terrain areas with significant water erosion, showing strong spatial agglomeration and geographical differentiation. In future climate scenarios, SOC stocks in each erosion zone show a decreasing trend, and it intensifies with different climate change scenarios (SSP245-SSP585) and time progression (2050–2090). For example, in the SSP585 scenario of 2090, the SOC stocks in the freeze–thaw erosion area decreased to 20.98 t ha^{-1}, a decrease of about 37.7% compared with the baseline period, indicating that this type of area is particularly sensitive to warming. The SOC stocks in the water erosion zone and wind erosion zone continue to be lost, but in absolute terms, the water erosion zone is still the main reserve of total SOC due to its large area. From the perspective of spatial variation, the attached figure further reveals the hotspots of SOC stocks changes: the freeze–thaw zone shows significant retreat, the middle and low latitudes of the water erosion zone show significant carbon loss, and the wind erosion zone maintains a relatively low level overall but is locally affected by precipitation patterns. This differential response not only confirms the differential feedback of different erosion processes on climate factors but also highlights the need to consider geographical and mechanistic heterogeneity in regional scale SOC stocks simulations.

TABLE 4 | Statistical analysis of soil organic carbon stocks across different erosion zones and climate scenarios.

Erosion type	Area (km^2)	Base period Mean (t ta^{-1})	Base period SOC stocks (Pg)	2050-SSP245 Mean (t ta^{-1})	2050-SSP245 SOC stocks (Pg)	2050-SSP585 Mean (t ta^{-1})	2050-SSP585 SOC stocks (Pg)	2090-SSP245 Mean (t ta^{-1})	2090-SSP245 SOC stocks (Pg)	2090-SSP585 Mean (t ta^{-1})	2090-SSP585 SOC stocks (Pg)
Water erosion	5.31×10^6	20.53	10.9	18.31	9.71	17.99	9.55	17.7	9.39	16.59	8.8
Wind erosion	2.28×10^6	10.47	2.39	8.96	2.04	8.92	2.04	8.92	2.04	8.47	1.93
Freeze–thaw erosion	1.84×10^6	33.69	6.2	24.47	4.5	24.15	4.44	23.74	4.37	20.98	3.86
Total	9.43×10^6	—	19.49	—	16.25	—	16.03	—	15.8	—	14.59

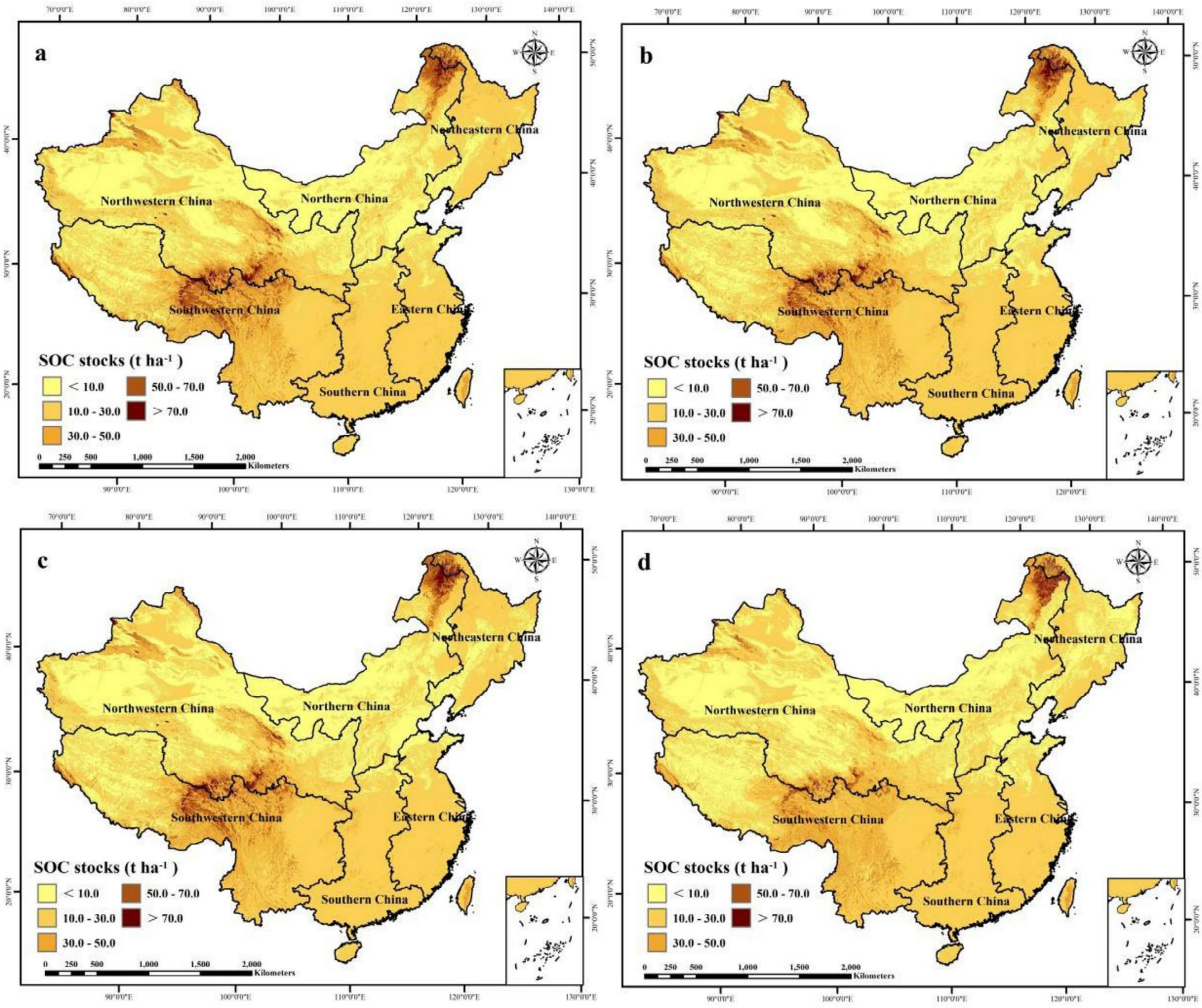

FIGURE 3 | Spatial distribution of soil organic carbon stocks under different climate scenarios in the future (a: SSP245 scenario in 2050; b: SSP585 scenario in 2050; c: SSP245 scenario in 2090; d: SSP585 scenario in 2090). Wiley acknowledges that the borders within the figure are subject to multiple territorial claims. [Colour figure can be viewed at wileyonlinelibrary.com]

4 | Discussion

4.1 | Effect of Environmental Factors Across Erosion Zones on SOC Stocks

In the water-eroded regions of China, environmental factors exerted a significant influence on topsoil SOC stocks, primarily through the integrated regulation of hydrothermal conditions and topographic factors (Figure 4). MAT and MAP accounted for 27.84% and 16.23% of the explained variation, respectively, emerging as dominant drivers. This highlights that the interaction between water and heat not only governs vegetation productivity and litter input but also profoundly regulates soil microbial activity and the rate of organic matter decomposition (Butenschoen

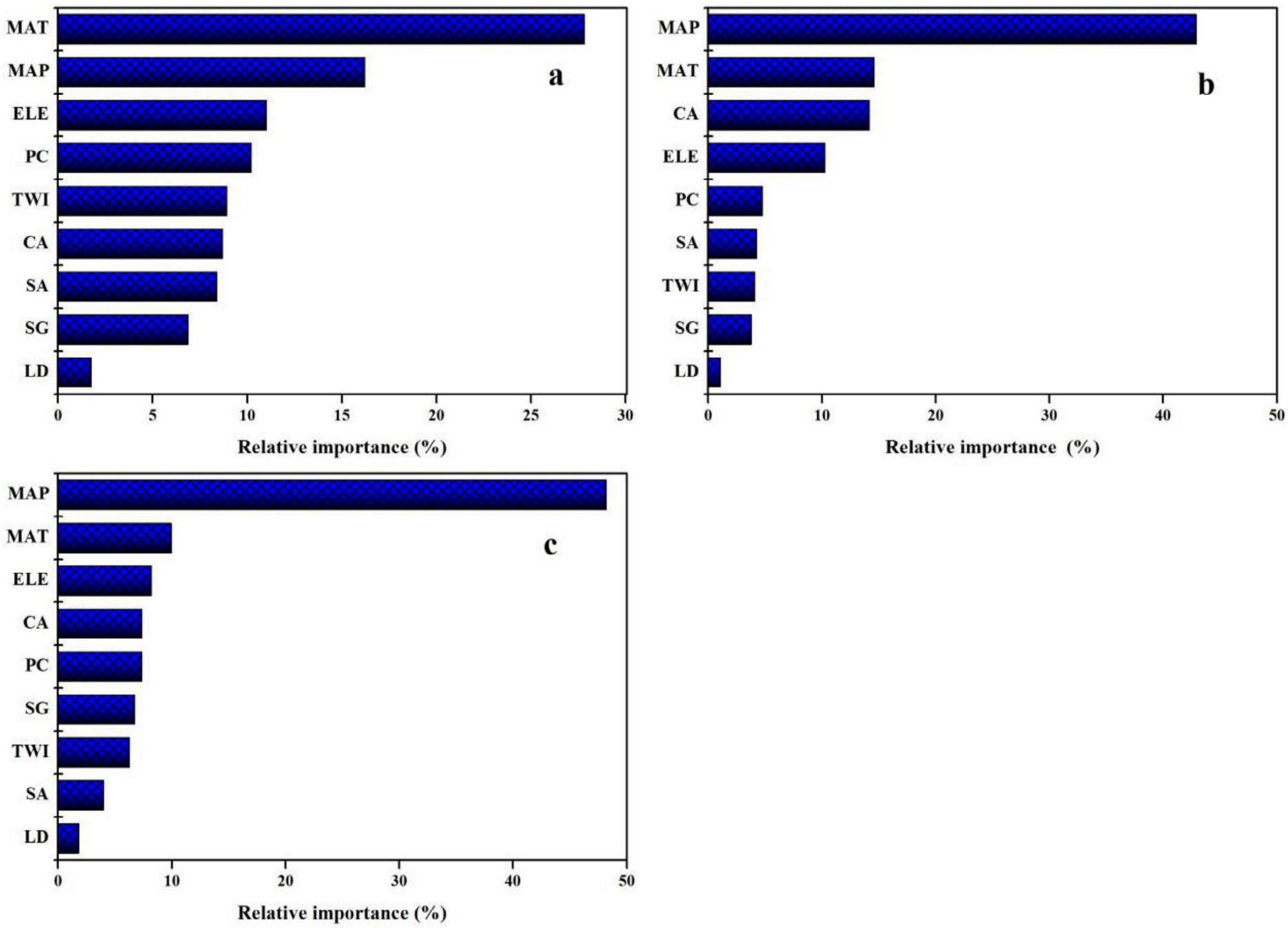

FIGURE 4 | Average relative importance of environmental factors in water erosion (a), wind erosion (b), and freeze–thaw erosion (c) areas, as predicted by 100 iterations of the LightGBM model. [Colour figure can be viewed at wileyonlinelibrary.com]

et al. 2011; Conant et al. 2011). High temperature combined with high humidity can accelerate the mineralization of organic carbon, whereas moderate hydrothermal conditions promote plant root development and humus formation (Demyanyuk et al. 2018; Li et al. 2023). Additionally, ELE and PC exerted significant influences, reflecting the role of topography in redistributing hydrological processes. Higher elevation areas typically experienced lower temperatures and slower decomposition of organic matter, which favors SOC accumulation (Blackburn et al. 2022; Adiyah et al. 2022). PC indirectly regulated the spatial distribution and stability of organic carbon by influencing surface runoff velocity and soil erosion intensity. Topographic factors, including SG, SA, CA, and TWI, collectively influence the spatial heterogeneity of soil moisture and nutrient distribution, thereby regulating the occurrence and stabilization of SOC stocks (Adhikari et al. 2019). Although the effect of LD was relatively minor compared with topographic factors, it remained significant—particularly in regions with intensive human activities. Vegetation cover and land management practices can alter soil structure and disrupt the balance of carbon inputs and outputs (Adiyah et al. 2022). Overall, SOC stocks in water-eroded areas is governed by multiple interacting environmental factors, such as climate, hydrothermal conditions, terrain-induced redistribution, and human activity disturbances. The dynamics of SOC exhibit distinct regional patterns and high ecological sensitivity.

In wind-eroded areas, the influence of environmental factors on topsoil SOC stocks was predominantly governed by water availability and its synergistic interactions with topographic and climatic factors. MAP emerged as the most critical determinant, with a relative importance of 42.91%, reinforcing the understanding that water availability is the primary limiting factor for ecosystem functioning and soil carbon sequestration in arid and semi-arid regions. Precipitation not only stimulates plant growth, thereby increasing aboveground litter and root-derived carbon inputs, but also enhances the physical protection of soil organic matter by improving soil aggregation and structure (Jobbágy and Jackson 2000; Beillouin et al. 2022). MAT exerts a certain influence on soil respiration and organic matter decomposition, with rising temperatures potentially accelerating carbon loss, particularly under conditions of water stress (Conant et al. 2011). CA, as a key topographic and hydrological parameter, reflects local runoff accumulation capacity and sedimentation processes. Its high explanatory power suggests that the spatial distribution of SOC stocks in wind-eroded regions is strongly shaped by the redistribution of sediment-associated organic matter (Adhikari et al. 2019; Wang, Bian, et al. 2025). ELE indirectly affects SOC content by modulating microclimatic conditions and vegetation patterns. Topographic attributes such as PC, SG, SA, and TWI collectively characterize the spatial distribution of surface energy and materials, thereby influencing wind erosion intensity and soil retention capacity (Zhou et al. 2020). Notably, LD exhibits a relatively minor influence, likely because natural drivers still dominate across extensive wind-eroded landscapes; however, human activity disturbances such as overgrazing and land reclamation may nonetheless intensify carbon depletion (Beillouin et al. 2022). Overall, SOC dynamics in wind-eroded areas follow a pattern of "water control, terrain modulation, and climatic coupling," reflecting the response mechanism of fragile ecosystem carbon cycling to climate change and surface geomorphological processes.

In the freeze–thaw erosion zone, environmental factors exert distinct influences on topsoil SOC stocks, underscoring the critical role of hydrothermal conditions and high-altitude topographic factors. MAP emerges as the dominant factor, with a relative importance of 48.20%, indicating that precipitation—particularly solid precipitation and the resulting snow cover—plays a central regulatory role in modulating soil temperature, moisture, and freeze–thaw dynamics. As an insulating layer, snow reduces soil freezing depth, thereby influencing microbial activity and the rate of organic matter decomposition (Wu 2020). Additionally, meltwater from snowpack sustains soil moisture during the growing season, thereby regulating vegetation productivity and carbon inputs to the soil (Brooks et al. 2011; Korup and Rixen 2014). MAT, contributing 9.96% relative importance, directly affects organic carbon stability by influencing the thickness of the active layer in permafrost regions and the frequency of freeze–thaw cycles. Warming temperatures may accelerate permafrost degradation, potentially triggering the remineralization of previously stabilized organic carbon pools (Kirschbaum 1995; Butenschoen et al. 2011). ELE, as a key coupling indicator of terrain and climate, not only governs temperature and precipitation patterns but also influences snow distribution and melt timing by modulating solar radiation and wind conditions, thereby regulating the intensity of freeze–thaw erosion and the spatial heterogeneity of SOC stocks (Zhou et al. 2020; Blackburn et al. 2022). CA, PC, SG, and TWI collectively characterize surface runoff pathways and material transport processes, shaping soil moisture regimes and the deposition and burial of organic matter. SA controls the spatial distribution of solar radiation, inducing variations in local thermal conditions that affect freeze–thaw cycles and carbon dynamics within vegetation–soil systems (Adiyah et al. 2022). Although LD exerts a relatively minor influence, it may amplify surface soil disturbance and carbon loss under grazing or engineering activities. Overall, SOC dynamics in freeze–thaw affected regions are governed by an integrated "precipitation–temperature–topography" system, exhibiting high sensitivity and potential irreversibility in response to climate warming and altered precipitation regimes. This makes them a critical component in understanding carbon balance in high-altitude ecosystems and their feedback to global environmental change.

4.2 | Response of SOC Stocks in Different Erosion Zones Under Future Climate Change

Based on the baseline data from 2018, there is a significant spatial differentiation in surface SOC stocks across different erosion zones in China, primarily driven by the synergistic effects of hydrothermal conditions, erosion types, and topographic characteristics. The freeze–thaw erosion zone exhibits the highest SOC stocks, which is closely linked to its unique high-altitude environment (Adhikari et al. 2019; Wang, Zhang, et al. 2025). The perennially low temperatures in this region suppress soil microbial activity and substantially reduce the decomposition rate of organic matter (Conant et al. 2011; Qi et al. 2016). At the same time, while extensive wetland and grassland vegetation have abundant litter input to soils, their SOC is significantly affected by frequent freeze–thaw cycles (Wu 2020). In contrast, the water erosion zone is predominantly located in the humid and semi-humid regions of eastern and southern China. High annual precipitation and temperature promote both vegetation growth and carbon input, but also accelerate the mineralization of organic matter (Naipal et al. 2018; Adeyeri et al. 2024). Moreover, intense water erosion leads to carbon loss via runoff, resulting in moderate SOC stocks (Polyakov and Lal 2004). The wind erosion zone encompasses extensive arid and semi-arid regions in northwestern China. Severe water scarcity constrains vegetation productivity, leading to reduced carbon inputs into the soil (Rockström and Barron 2007). Concurrently, intense wind erosion accelerates the removal of topsoil SOC, keeping carbon stocks at consistently low levels (Zhou et al. 2020). The spatial pattern of carbon stocks closely mirrors the environmental gradients characteristic of China's natural landscape. As temperature and precipitation decline from the southeast to the northwest, the dominant erosion mechanism shifts from water erosion to wind erosion and freeze–thaw erosion, accompanied by systematic variations in SOC stocks.

In future climate change scenarios, SOC stocks across all erosion zones exhibit a declining trend, with losses becoming increasingly pronounced under intensified greenhouse gas emission scenarios and over time, highlighting the significant impact of climate change on terrestrial carbon pools (Figure 3). The freeze–thaw erosion zone is particularly sensitive to warming, and under the SSP585 scenario by 2090, its organic carbon stocks are projected to decline by ~37.7%. This reduction is primarily attributed to permafrost degradation induced by rising temperatures, which deepens the active layer and exposes previously sequestered ancient organic carbon to microbial decomposition, thereby accelerating carbon release (Brooks et al. 2011; Wu 2020). Additionally, altered snow cover patterns and intensified freeze–thaw cycles can compromise soil structure, further enhancing carbon emissions (Bonfanti et al. 2025). As the largest erosion-affected region in China, the water erosion zone experiences the greatest absolute loss in carbon stocks, thus exerting the most substantial influence on the nation's total soil carbon pool (Table 4). Changes in future precipitation patterns, such as increased intensity and uneven distribution, may exacerbate soil erosion, losing particulate organic carbon (Polyakov and Lal 2004). Concurrently, rising temperatures are expected to increase soil respiration rates. SOC stocks in wind-eroded regions are projected to decline gradually, although the magnitude of this change remains relatively small, likely due to the region's inherently low carbon pool background levels. The dynamics of carbon stocks in these areas are primarily governed by precipitation changes. A slight increase in precipitation could promote local vegetation recovery and enhance carbon sequestration, whereas intensified drought conditions may further suppress vegetation growth and amplify wind erosion, thereby accelerating carbon loss (Adhikari et al. 2019; Adeyeri et al. 2024; Wang, Bian, et al. 2025).

From a spatial perspective, future changes in SOC stocks in China are projected to exhibit distinct hotspot regions (Figure 3). The freeze–thaw erosion zone is likely to undergo significant spatial contraction, particularly at the periphery of the Qinghai Tibet Plateau region, where sharp declines in carbon stocks will form the primary hotspots of carbon loss. The water erosion zone, particularly the hilly and mountainous regions at mid to low latitudes, is expected to become a significant area for carbon loss due to accelerated organic matter decomposition from rising temperatures and increased frequency of extreme precipitation events that intensify soil erosion (Maïga-Yaleu et al. 2013; Naipal et al. 2018). Within the wind erosion zone, more complex patterns may emerge, and carbon stocks in certain local areas may exhibit a stable or even slightly increasing trend due to altered precipitation patterns. This differentiated response not only confirms the distinct feedback mechanisms of climate factors across various erosion processes but also underscores the necessity of accounting for geographical and mechanistic heterogeneity in predicting and managing future soil carbon dynamics (Adhikari et al. 2019; Wang et al. 2023; Haghighi et al. 2025). The findings indicate that climate change could substantially alter the carbon sink capacity of China's terrestrial ecosystems by modifying erosion intensity and spatial patterns (Yan et al. 2005; Wan et al. 2011; Naipal et al. 2018). Consequently, the development of ecological conservation and climate change adaptation strategies must prioritize precise, region-specific management approaches—such as monitoring permafrost degradation in freeze–thaw regions, enhancing soil and water conservation infrastructure in areas prone to water erosion, and optimizing vegetation restoration practices in wind-erosion-dominated zones—to mitigate soil carbon loss and sustain ecosystem carbon sink stability.

4.3 | Limitations in Current Study

This study selected LightGBM as the optimal model for simulating the spatial distribution of SOC stocks across different erosion zones in China, based on its high R^2 and LCCC values, as well as low MAE and RMSE. Although the model demonstrates robust overall performance, several sources of uncertainty in the prediction process must be carefully considered when interpreting results and informing decision-making.

Firstly, although the soil samples used for modeling were collected and analyzed in 2020 by multiple teams following standardized protocols, systematic errors arising from instrument calibration discrepancies, variations in laboratory microenvironments, or operator subjectivity cannot be entirely ruled out. While standardized procedures help mitigate some of these issues, at a national scale, differences in sampling timing, stocks conditions, and measurement batches across regions may still compromise data consistency (Wang, Bian, et al. 2025). This variability can impair the accuracy of model parameter estimation, particularly in ecotones or areas with complex topography, where insufficient sample representativeness may further amplify uncertainty (Navarro et al. 2024).

Secondly, environmental factors data are derived from multiple reanalysis datasets that vary in original spatial resolution, observation mechanisms, and coordinate systems. Although spatial registration and resampling were conducted using the ArcGIS 10.2 platform to achieve grid uniformity, these preprocessing steps may result in localized information loss or introduce smoothing effects—particularly in regions with pronounced terrain undulations and complex land cover patterns (Freitag et al. 2018). For instance, topographic factors such as SG and SA may lose their ecological representativeness after resampling, while high-frequency variations in vegetation indices or surface moisture within heterogeneous landscapes are often inadequately retained. This can compromise the accuracy of model fitting between environmental predictors and SOC stocks, thereby introducing potential biases in spatial extrapolation.

Thirdly, the inconsistency among climate data sources introduces significant uncertainty into predictions. Historical climate data are primarily derived from station observations and reanalysis products, whereas future climate scenarios depend on downscaled outputs from global climate models. These downscaled models exhibit considerable biases in simulating regional precipitation patterns, extreme temperature events, seasonal droughts, rainstorms, and other critical climate variables, and they often lack adequate spatial coherence across different climatic factors (Adhikari et al. 2019; Wang, Zhang, et al. 2025). Such systematic biases can directly influence the representation of hydrothermal conditions driving SOC dynamics, particularly in regions sensitive to precipitation fluctuations, such as wind erosion zones, and areas highly sensitive to temperature changes, such as freeze–thaw regions. Consequently, the uncertainty inherent in climate data substantially undermines the model's predictive capability for future SOC dynamics.

Fourthly, the model construction is based on the current soil environmental conditions and does not fully account for the potential impacts of future human activities and natural system evolution on SOC stocks. For instance, land use patterns may shift in response to policy changes or economic development; agricultural management practices—such as straw return and organic fertilizer application—may be widely adopted to enhance carbon sequestration; and vegetation restoration initiatives or urbanization processes could significantly alter carbon inputs and erosion rates. Since the current model does not integrate these dynamic factors, its static assumptions may increasingly diverge from real-world system behavior over time, thereby limiting its predictive reliability and applicability under changing environmental and socioeconomic scenarios.

Finally, this study focused exclusively on SOC stocks in the topsoil layer (0–30 cm) and did not assess the deep soil carbon pool. While surface soil carbon is more responsive to external environmental changes, deep soil layers (e.g., 30–100 cm) contain substantial amounts of stable organic carbon and can actively participate in carbon cycling under certain conditions. Ignoring the dynamics of deep soil carbon may result in an incomplete evaluation of regional soil carbon sequestration potential, particularly in ecosystems characterized by deep-rooted vegetation or susceptible to deep carbon mobilization. This limitation underscores the need for caution when extrapolating the findings to broader contexts, as it may affect the comprehensiveness and robustness of the overall conclusions.

Despite the aforementioned uncertainties, simulating the future dynamics of SOC under various socio-economic development pathways in this study retains substantial scientific value and policy relevance. The findings offer a critical foundation for formulating differentiated soil conservation strategies, designing ecological compensation mechanisms, and optimizing regional carbon neutrality trajectories—particularly within national efforts to address climate change and advance sustainable land management. These projections provide policymakers with clear, spatially explicit, and scenario-based scientific guidance.

5 | Conclusions

This study uses the LightGBM model to systematically simulate the spatial distribution and dynamics of surface SOC stocks across three major erosion types in China including water erosion, wind erosion, and freeze–thaw erosion areas under future climate scenarios. The results indicate that current SOC stocks in China exhibit pronounced spatial heterogeneity, with the highest organic carbon stocks observed in freeze–thaw erosion areas, followed by water erosion areas, and the lowest in wind erosion areas. This spatial pattern is primarily governed by the synergistic effects of hydrothermal conditions and topographic factors. The model identifies annual mean temperature, annual precipitation, and elevation as the key environmental drivers influencing the spatial variability of SOC stocks. Their relative importance varies significantly across different erosion types, highlighting a complex regulatory mechanism through which climate and terrain jointly modulate carbon cycling processes. Future scenario projections indicate that under both the SSP2-4.5 and SSP5-8.5 pathways, SOC stocks in erosion-prone regions across China exhibit a declining trend, which intensifies with increasing greenhouse gas emissions over time. The freeze–thaw erosion zone is particularly sensitive to climate change, with organic carbon stocks projected to decrease by 37.7% under the SSP5-8.5 scenario by 2090, highlighting the high vulnerability of the carbon pool in China to rising temperatures. Although carbon loss per unit area in water-eroded regions is relatively low, their extensive spatial distribution makes them the primary contributors to total SOC loss in China. Spatially, carbon loss hotspots are predominantly concentrated in the retreat zones of freeze–thaw regions and mid to low-latitude water erosion zones, whereas changes in wind-eroded areas are comparatively moderate but significantly influenced by shifts in precipitation patterns. These findings reveal pronounced regional and mechanistic heterogeneity in how Chinese soils respond to future climate change, underscoring the necessity of incorporating site-specific natural conditions and carbon cycling dynamics of different erosion types into national soil conservation and carbon neutrality strategies. To promote sustainable management of soil carbon stocks, we recommend enhancing soil and water conservation practices and agricultural management in water-eroded areas, optimizing vegetation restoration and water resource use in wind-eroded regions, and strengthening permafrost monitoring and ecological regulation in freeze–thaw zones—collectively improving the resilience and carbon sequestration capacity of Chinese terrestrial ecosystems under a changing climate.

Funding

This work was supported by the National Key R&D Program of China (Grant No. 2023YFD1501300), National Science Foundation of China (Grant No. 42207289), Natural Science Foundation of Jilin Province (Grant No. YDZJ202401480ZYTS), Project of Liaoning Provincial Department of Science and Technology (Grant No. 2025-MSLH-612).

Data Availability Statement

The data that support the findings of this study are available on request from the corresponding author. The data are not publicly available due to privacy or ethical restrictions.

References

Adeyeri, O. E., A. H. Folorunsho, T. E. Adeliyi, et al. 2024. "Climate Change Is Intensifying Rainfall Erosivity and Soil Erosion in West Africa." *Science of the Total Environment* 955: 177174.

Adhikari, K., P. R. Owens, Z. Libohova, D. M. Miller, S. A. Wills, and J. Nemecek. 2019. "Assessing Soil Organic Carbon Stock of Wisconsin, USA and Its Fate Under Future Land Use and Climate Change." *Science of the Total Environment* 667: 833–845.

Adiyah, F., E. Michéli, A. Csorba, et al. 2022. "Effects of Landuse Change and Topography on the Quantity and Distribution of Soil Organic Carbon Stocks on Acrisol Catenas in Tropical Small-Scale Shade Cocoa Systems of the Ashanti Region of Ghana." *Catena* 216: 106366.

Beillouin, D., R. Cardinael, D. Berre, et al. 2022. "A Global Overview of Studies About Land Management, Land-Use Change, and Climate Change Effects on Soil Organic Carbon." *Global Change Biology* 28, no. 4: 1690–1702.

Berhe, A. A., R. T. Barnes, J. Six, and E. Marín-Spiotta. 2018. "Role of Soil Erosion in Biogeochemical Cycling of Essential Elements: Carbon, Nitrogen, and Phosphorus." *Annual Review of Earth and Planetary Sciences* 46, no. 1: 521–548.

Bishop, T. F. A., A. B. McBratney, and G. M. Laslett. 1999. "Modelling Soil Attribute Depth Functions With Equal-Area Quadratic Smoothing Splines." *Geoderma* 91, no. 1–2: 27–45.

Blackburn, K. W., Z. Libohova, K. Adhikari, C. Kome, X. Maness, and M. R. Silman. 2022. "Influence of Land Use and Topographic Factors on Soil Organic Carbon Stocks and Their Spatial and Vertical Distribution." *Remote Sensing* 14, no. 12: 2846.

Bonfanti, N., J. Poulenard, J. C. Clement, et al. 2025. "Influence of Snow Cover and Microclimate on Soil Organic Carbon Stability in European Mountain Grasslands." *Catena* 250: 108744.

Bonfatti, B. R., A. E. Hartemink, and E. Giasson. 2016. "Comparing Soil C Stocks From Soil Profile Data Using Four Different Methods." In *Digital Soil Morphometrics*, 315–329. Springer International Publishing.

Borrelli, P., C. Alewell, P. Alvarez, et al. 2021. "Soil Erosion Modelling: A Global Review and Statistical Analysis." *Science of the Total Environment* 780: 146494.

Breiman, L. 2001. "Random Forests." *Machine Learning* 45, no. 1: 5–32.

Brooks, P. D., P. Grogan, P. H. Templer, P. Groffman, M. G. Öquist, and J. Schimel. 2011. "Carbon and Nitrogen Cycling in Snow-Covered Environments." *Geography Compass* 5, no. 9: 682–699.

Butenschoen, O., S. Scheu, and N. Eisenhauer. 2011. "Interactive Effects of Warming, Soil Humidity and Plant Diversity on Litter Decomposition and Microbial Activity." *Soil Biology and Biochemistry* 43, no. 9: 1902–1907.

Carmona, P., F. Climent, and A. Momparler. 2019. "Predicting Failure in the US Banking Sector: An Extreme Gradient Boosting Approach." *International Review of Economics and Finance* 61: 304–323.

Chappell, A., J. Baldock, and J. Sanderman. 2016. "The Global Significance of Omitting Soil Erosion From Soil Organic Carbon Cycling Schemes." *Nature Climate Change* 6, no. 2: 187–191.

Chen, T., T. He, M. Benesty, et al. 2015. "Xgboost: Extreme Gradient Boosting." R Package Version 0.4-2, 1(4), pp.1–4.

Conant, R. T., M. G. Ryan, G. I. Ågren, et al. 2011. "Temperature and Soil Organic Matter Decomposition Rates–Synthesis of Current Knowledge and a Way Forward." *Global Change Biology* 17, no. 11: 3392–3404.

de Nijs, E. A., and E. L. Cammeraat. 2020. "The Stability and Fate of Soil Organic Carbon During the Transport Phase of Soil Erosion." *Earth-Science Reviews* 201: p.103067.

Demyanyuk, O. S., O. V. Sherstoboeva, A. A. Bunas, and O. V. Dmitrenko. 2018. "Effects of Different Fertilizer Systems and Hydrothermal Factors on Microbial Activity in the Chernozem in Ukraine." *Biosystems Diversity* 26, no. 4: 309–315.

Doetterl, S., A. A. Berhe, K. Heckman, et al. 2025. "A Landscape-Scale View of Soil Organic Matter Dynamics." *Nature Reviews Earth & Environment* 6, no. 1: 67–81.

Freitag, B. M., U. S. Nair, and D. Niyogi. 2018. "Urban Modification of Convection and Rainfall in Complex Terrain." *Geophysical Research Letters* 45, no. 5: 2507–2515.

Gao, J., C. Shi, J. Yang, H. Yue, Y. Liu, and B. Chen. 2023. "Analysis of Spatiotemporal Heterogeneity and Influencing Factors of Soil Erosion in a Typical Erosion Zone of the Southern Red Soil Region, China." *Ecological Indicators* 154: 110590.

Guan, Y. 2025. "Ethnogeography in China." In *Theoretical Study of Ethnogeography*, 261–355. Springer Nature Singapore.

Guo, J., S. Yun, Y. Meng, et al. 2023. "Prediction of Heating and Cooling Loads Based on Light Gradient Boosting Machine Algorithms." *Building and Environment* 236: 110252.

Guo, L., R. Liu, C. Men, et al. 2021. "Multiscale Spatiotemporal Characteristics of Landscape Patterns, Hotspots, and Influencing Factors for Soil Erosion." *Science of the Total Environment* 779: 146474.

Haghighi, P., S. M. Soleimanpour, and A. Moradi. 2025. "The Effects of Climate Change on Precipitation and Temperature Using SSP Scenarios (Case Study: Fars Province)." *Water and Soil Management and Modelling* 5, no. 2: 199–218.

Hancock, G. R., V. Kunkel, T. Wells, and C. Martinez. 2019. "Soil Organic Carbon and Soil Erosion–Understanding Change at the Large Catchment Scale." *Geoderma* 343: 60–71.

Hindarto, D. 2024. "Case Study: Gradient Boosting Machine vs Light GBM in Potential Landslide Detection." *Journal of Computer Networks, Architecture and High Performance Computing* 6, no. 1: 169–178.

Hunter, B. D., J. J. Roering, L. C. Silva, and K. C. Moreland. 2024. "Geomorphic Controls on the Abundance and Persistence of Soil Organic Carbon Pools in Erosional Landscapes." *Nature Geoscience* 17, no. 2: 151–157.

Jobbágy, E. G., and R. B. Jackson. 2000. "The Vertical Distribution of Soil Organic Carbon and Its Relation to Climate and Vegetation." *Ecological Applications* 10, no. 2: 423–436. Curran Associates, Inc.

Ke, G., Q. Meng, T. Finley, et al. 2017. "Lightgbm: A Highly Efficient Gradient Boosting Decision Tree." In *Advances in Neural Information Processing Systems*, vol. 30.

Kirschbaum, M. U. 1995. "The Temperature Dependence of Soil Organic Matter Decomposition, and the Effect of Global Warming on Soil Organic C Storage." *Soil Biology & Biochemistry* 27, no. 6: 753–760.

Korup, O., and C. Rixen. 2014. "Soil Erosion and Organic Carbon Export by Wet Snow Avalanches." *Cryosphere* 8, no. 2: 651–658.

Lal, R. 2003. "Soil Erosion and the Global Carbon Budget." *Environment International* 29, no. 4: 437–450.

Lal, R. 2004. "Soil Carbon Sequestration Impacts on Global Climate Change and Food Security." *Science* 304, no. 5677: 1623–1627.

Lal, R. 2005. "Soil Erosion and Carbon Dynamics." *Soil and Tillage Research* 81, no. 2: 137–142.

Li, Q., L. Wang, Y. Fu, et al. 2023. "Transformation of Soil Organic Matter Subjected to Environmental Disturbance and Preservation of Organic Matter Bound to Soil Minerals: A Review." *Journal of Soils and Sediments* 23, no. 3: 1485–1500.

Lin, H., X. Duan, Y. Li, L. Zhang, L. Rong, and R. Li. 2022. "Simulating the Effects of Erosion on Organic Carbon Dynamics in Agricultural Soils." *Catena* 208: 105753.

Lin, L. 1989. "A Concordance Correlation Coefficient to Evaluate Reproducibility." *Biometrics* 45: 255–268.

Liu, S., N. Bliss, E. Sundquist, and T. G. Huntington. 2003. "Modeling Carbon Dynamics in Vegetation and Soil Under the Impact of Soil Erosion and Deposition." *Global Biogeochemical Cycles* 17, no. 2: 1074.

Maïga-Yaleu, S., I. Guiguemde, H. Yacouba, et al. 2013. "Soil Crusting Impact on Soil Organic Carbon Losses by Water Erosion." *Catena* 107: 26–34.

Matejovic, I. 1993. "Determination of Carbon, Hydrogen, and Nitrogen in Soils by Automated Elemental Analysis (Dry Combustion Method)." *Communications in Soil Science and Plant Analysis* 24, no. 17–18: 2213–2222.

McBratney, A. B., M. M. Santos, and B. Minasny. 2003. "On Digital Soil Mapping." *Geoderma* 117, no. 1–2: 3–52.

Nabiollahi, K., S. Eskandari, R. Taghizadeh-Mehrjardi, R. Kerry, and J. Triantafilis. 2019. "Assessing Soil Organic Carbon Stocks Under Land-Use Change Scenarios Using Random Forest Models." *Carbon Management* 10, no. 1: 63–77.

Naipal, V., P. Ciais, Y. Wang, R. Lauerwald, B. Guenet, and K. Van Oost. 2018. "Global Soil Organic Carbon Removal by Water Erosion Under Climate Change and Land Use Change During AD 1850–2005." *Biogeosciences* 15, no. 14: 4459–4480.

Navarro, A., G. Lee, R. Martín, and F. J. Tapiador. 2024. "Uncertainties in Measuring Precipitation Hinders Precise Evaluation of Loss of Diversity in Biomes and Ecotones." *Npj Climate and Atmospheric Science* 7, no. 1: p.35.

Odgers, N. P., Z. Libohova, and J. A. Thompson. 2012. "Equal-Area Spline Functions Applied to a Legacy Soil Database to Create Weighted-Means Maps of Soil Organic Carbon at a Continental Scale." *Geoderma* 189: 153–163.

Olson, K. R., M. Al-Kaisi, R. Lal, and L. Cihacek. 2016. "Impact of Soil Erosion on Soil Organic Carbon Stocks." *Journal of Soil and Water Conservation* 71, no. 3: 61A–67A.

Polyakov, V., and R. Lal. 2004. "Modeling Soil Organic Matter Dynamics as Affected by Soil Water Erosion." *Environment International* 30, no. 4: 547–556.

Qi, R., J. Li, Z. Lin, et al. 2016. "Temperature Effects on Soil Organic Carbon, Soil Labile Organic Carbon Fractions, and Soil Enzyme Activities Under Long-Term Fertilization Regimes." *Applied Soil Ecology* 102: 36–45.

R Development Core Team. 2013. *R: A Language and Environment for Statistical Computing*. R Foundation for Statistical Computing. https://www.rproject.org/.

Reyes Rojas, L. A., K. Adhikari, and S. J. Ventura. 2018. "Projecting Soil Organic Carbon Distribution in Central Chile Under Future Climate Scenarios." *Journal of Environmental Quality* 47, no. 4: 735–745.

Rockström, J., and J. Barron. 2007. "Water Productivity in Rainfed Systems: Overview of Challenges and Analysis of Opportunities in Water Scarcity Prone Savannahs." *Irrigation Science* 25, no. 3: 299–311.

Sibindi, R., R. W. Mwangi, and A. G. Waititu. 2023. "A Boosting Ensemble Learning Based Hybrid Light Gradient Boosting Machine and Extreme Gradient Boosting Model for Predicting House Prices." *Engineering Reports* 5, no. 4: e12599.

Wan, Y., E. Lin, W. Xiong, Y. E. Li, and L. Guo. 2011. "Modeling the Impact of Climate Change on Soil Organic Carbon Stock in Upland Soils in the 21st Century in China." *Agriculture, Ecosystems & Environment* 141, no. 1–2: 23–31.

Wang, S., S. Bian, Z. Wang, et al. 2025. "Three-Dimensional Modeling of Soil Organic Carbon Stocks in Forest Ecosystems of Northeastern China Under Future Climate Warming Scenarios." *Forests* 16, no. 8: p.1209.

Wang, S., X. Zhang, K. Adhikari, et al. 2023. "Impact of Future Climate Warming on Soil Organic Carbon Stocks in Inner Mongolia, China." *Ecological Indicators* 156: p.111208.

Wang, S., X. Zhang, Q. Zhuang, et al. 2025. "Spatio-Temporal Variations in Soil Organic Carbon Stocks in Different Erosion Zones of Cultivated Land in Northeast China Under Future Climate Change Conditions." *Agronomy* 15, no. 11: 2459.

Wiesmeier, M., F. Barthold, B. Blank, and I. Kögel-Knabner. 2011. "Digital Mapping of Soil Organic Matter Stocks Using Random Forest Modeling in a Semi-Arid Steppe Ecosystem." *Plant and Soil* 340, no. 1: 7–24.

Wu, Q. 2020. "Season-Dependent Effect of Snow Depth on Soil Microbial Biomass and Enzyme Activity in a Temperate Forest in Northeast China." *Catena* 195: 104760.

Yan, H., S. Wang, C. Wang, G. Zhang, and N. Patel. 2005. "Losses of Soil Organic Carbon Under Wind Erosion in China." *Global Change Biology* 11, no. 5: 828–840.

Zheng, H., C. Miao, C. Huntingford, et al. 2025. "The Impacts of Erosion on the Carbon Cycle." *Reviews of Geophysics* 63, no. 1: p.e2023RG000829.

Zhou, Z., Z. Zhang, X. Zou, K. Zhang, and W. Zhang. 2020. "Quantifying Wind Erosion at Landscape Scale in a Temperate Grassland: Nonignorable Influence of Topography." *Geomorphology* 370: 107401.